New members of the [Mn6/oxime] family and analogues with converging [Mn3] planes

New members of the [Mn_6/oxime] family and novel analogues with converging [Mn_3] planes.

ANDREAS G. FLAMOURAKIS †, DIMITRIS A. KALOFOLIAS †, MILOSZ SICZEK ‡, TADEUSZ LIS ‡, EUAN K. BRECHIN*§ and CONSTANTINOS J. MILIOS*†

† Department of Chemistry, University of Crete, Voutes 71003, Herakleion, Greece.

‡ Faculty of Chemistry, University of Wroclaw, Joliot-Curie 14, Wroclaw 50-383, Poland.

§ EaStCHEM School of Chemistry, The University of Edinburgh, David Brewster Road, Edinburgh, EH9 3FJ, UK.

*Corresponding authors: E-mail: komil@chemistry.uoc.gr (C. J. Milios).

ebrechin@ed.ac.uk (E. K. Brechin)

Abstract

The synthesis, structural and magnetic characterization of five new members of the hexanuclear oximate [Mn^{III}_6] family is reported. All five clusters can be described with the general formula [$Mn^{III}_6O_2$(R-sao)$_6$(R'-CO_2)$_2$(sol)$_x$(H_2O)$_y$] (where R-saoH_2 = salicylaldoxime substituted at the oximic carbon atom with R = H, Me and Et; R' = 1-naphthalene, 2-naphthalene and 1-pyrene; sol = MeOH, EtOH or MeCN; x = 0-4 and y = 0-4). More specifically, the reaction of $Mn(ClO_4)_2 \cdot 6H_2O$ with salicylaldoxime-like ligands and the appropriate carboxylic acid in alcoholic or MeCN solutions in the presence of base afforded complexes **1**-**5**: [Mn_6O_2(Me-sao)$_6$(1-naphth-CO_2)$_2$(H_2O)(MeCN)]·4MeCN (**1**·4MeCN); [Mn_6O_2(Me-sao)$_6$(2-naphth-CO_2)$_2$(H_2O)(MeCN)]·3MeCN·0.1H_2O (**2**·3MeCN·0.1H_2O); [Mn_6O_2(Et-sao)$_6$(2-naphth-CO_2)$_2$(EtOH)$_4$(H_2O)$_2$] (**3**); [Mn_6O_2(Et-sao)$_6$(2-naphth-CO_2)$_2$(MeOH)$_6$] (**4**) and [Mn_6O_2(sao)$_6$(1-pyrene-CO_2)$_2$(H_2O)$_2$(EtOH)$_2$]·6EtOH (**5**·6EtOH). Clusters **3**, **4** and **5** display the usual [Mn_6/oximate] structural motif consisting of two [Mn_3O] sub-units bridged by two $O_{oximate}$ atoms from two R-sao^{2-} ligands to form the hexanuclear complex in which the two triangular [Mn_3] units are parallel to each other. On the contrary, clusters **1** and **2** display a highly distorted stacking arrangement of the two [Mn_3] sub-units resulting in two converging planes, thus forming a novel motif in the [Mn_6] family. Investigation of the magnetic properties for all complexes reveal dominant antiferromagnetic interactions for complexes **1**, **2** and **5**, while complexes **3** and **4** display dominant ferromagnetic interactions with a ground state of S = 12 for both clusters. Finally, complexes **3** and **4** display Single-Molecule Magnet behaviour with U_{eff} = 63 K and 36 K, respectively.

Keywords: Mn(III) oximate complexes; Converging [Mn_3] planes; Magnetic properties; Single-Molecule Magnets.

Figure for the table of contents

1. Introduction

Since the discovery of the Single Molecule Magnetism (SMM) phenomenon in the mixed-valence dodedanuclear manganese cluster $[Mn^{IV}_4Mn^{III}_8O_{12}(MeCO_2)_{16}(H_2O)_4]\cdot 2MeCO_2H\cdot 4H_2O$ [1-5], numerous paramagnetic polymetallic clusters that can retain their magnetization at low temperatures once magnetized upon removal of the external stimuli have been reported [6-22]. This unique magnetic behaviour results from the combination of a large spin ground state, and a relatively large and negative magnetoanisotropy, D, which creates a significant energy barrier to magnetization reversal, U, whose upper limit is given by $U= S^2 \left| D \right|$ for integer spin, and $U= (S^2\text{-}1/4) \left| D \right|$ for half-integer spin ground states. Besides the scientific interest that such molecules possess, it has been proposed that they may be used in various technological applications, such as in computer magnetic storage, in magnetic resonance imaging as contrast agents, and in cooling processes [23, 24]. Manganese oximate cluster chemistry has afforded a large family of compounds that function as SMMs; a series of complexes with general formulae $[Mn^{III}_xO_2(R\text{-}sao)_x(O_2CR)_{1\text{-}2}(L)_{4\text{-}6}]$ (R= H, Me, Et, Ph, etc; L= solvent and x = 3 or 6) were synthesized and characterized [25-39], with two representative members of this family that function as SMMs being $[Mn^{III}_6O_2(Et\text{-}sao)_6(O_2CPh)_2(EtOH)_4(H_2O)_2]$ [40] and $[Mn^{III}_6O_2(Et\text{-}sao)_6(O_2CPH(Me)_2)_2(EtOH)_6]$ [41]. A magneto-structural correlation was developed for this family of complexes in order to explain the "switch" from antiferromagnetic (AF) to ferromagnetic (F) exchange between neighbouring Mn centres, with the governing factor being the Mn-N-O-Mn torsion angle, τ [30]. According to this magnetostructural correlation there is a "magic area" of ~ 30.4-31.3°; τ angles of <30.4° lead to an AF (J<0) nearest-neighbour interaction, while for τ > 31.3° a F (J>0) interaction is achieved. The Mn-N-O-Mn torsion angle is affected both by the steric bulk of substituents of the oxime and carboxylate ligands, and as such, different combinations of R-saoH_2 and carboxylate ligands afford species with different torsion angles, and thus different magnetic properties.

In this contribution, we report seven new $[Mn^{III}_6$/oxime] compounds from the use of R-saoH_2 (R = H, Me, Et) and various carboxylic acids in Mn(III) chemistry. Two clusters of the family display a novel arrangement of the metallic core, in which the two $[Mn_3O]$ sub-units that form the hexanuclear core are positioned in a non-parallel fashion, while

in addition one μ_4-oxo group is present, in contrast with all other [Mn_6] complexes reported so far.

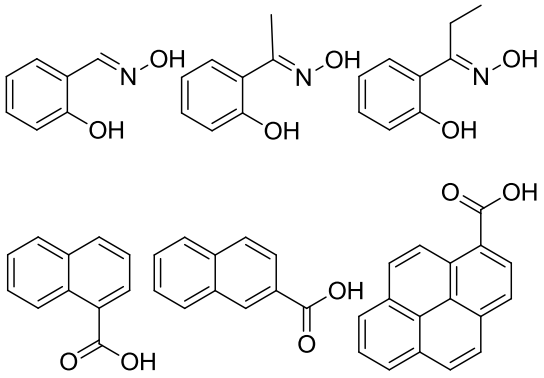

Scheme 1. Ligands discussed in the text; Top-left to bottom-right: $saoH_2$, Me-$saoH_2$, Et-$saoH_2$, 1-naphthoic acid, 2-naphthoic acid and 1-pyrene carboxylic acid.

2. Experimental

2.1. General and physical measurements

All manipulations were performed under aerobic conditions, using materials as received. Me-$saoH_2$, Et-$saoH_2$ and $saoH_2$ were synthesized by the reaction of the appropriate precursor aldehyde with hydroxylamine and sodium acetate in EtOH, as described in literature [42]. Elemental analyses (C, H, N) were performed by the University of Ioannina microanalysis service. Variable-temperature, solid-state direct current (dc) magnetic susceptibility data down to 5 K were collected on a Quantum Design MPMS-XL SQUID magnetometer equipped with a 7 T dc magnet at UoC. Diamagnetic corrections were applied to the observed paramagnetic susceptibilities using Pascal's constants.

2.2. Compound preparation

2.2.1. General synthetic strategy for 3, 4 and 5.

To pale pink solutions of $Mn(ClO_4)_2{\cdot}6H_2O$ in MeOH (or EtOH) were added equimolar amounts of the corresponding oxime and carboxylic acid ligands, in the presence of

excess base, NEt_3. The solutions were left stirring for ~30 min, filtered and then left to slowly evaporate. In each case suitable single-crystals grew after a period of 3-5 days. Anal. Calcd. $[Mn_6O_2(Et\text{-}sao)_6(2\text{-}naphthoic)_2(EtOH)_4(H_2O)_2]$ (**3**) ($C_{84}H_{96}Mn_6N_6O_{24}$): C 53.01, H 5.08, N 4.42 %. Found C 52.92, H 4.88, N 4.29 %. Anal. Calcd for $[Mn_6O_2(Et\text{-}sao)_6(2\text{-}naphthoic)_2(EtOH)_6]$ (**4**) ($C_{82}H_{92}Mn_6N_6O_{24}$): C 52.52, H 4.94, N 4.48 %. Found C 52.45, H 4.81, N 4.32 %. Anal. Calcd. for $[Mn_6O_2(sao)_6(1\text{-}pyrene)_2(H_2O)_2(EtOH)_2]\cdot 6EtOH$ (**5**·6EtOH) ($C_{92}H_{94}Mn_6N_6O_{28}$): C 53.60, H 4.60, N 4.08 %. Found C 53.48, H 4.37, N 3.95 %.

2.2.2. General synthetic strategy for 1 and 2.

To pale pink solutions of $Mn(ClO_4)_2\cdot 6H_2O$ in MeCN were added equimolar amounts of the derivitized oximes, the corresponding carboxylic acid and CH_3ONa. The solutions were left stirring for ~45 min, filtered and then left to slowly evaporate. In each case suitable crystals grew after a period of 3-5 days. Anal. Calcd. for $[Mn_6O_2(Me\text{-}sao)_6(1\text{-}naphthoic)_2(H_2O)(MeCN)]\cdot 4MeCN$ (**1**·4MeCN) ($C_{80}H_{73}Mn_6N_{11}O_{19}$): C 52.73, H 4.04, N 8.46%. Found C 52.60, H 3.82, N 8.29 %. Anal. Calcd. for $[Mn_6O_2(Me\text{-}sao)_6(2\text{-}naphthoic)_2(H_2O)(MeCN)]\cdot 3MeCN\cdot 0.1H_2O$ (**2**·3MeCN·0.1H_2O) ($C_{78}H_{70}Mn_6N_{10}O_{19}$): C 52.60, H 3.96, N 7.86%. Found C 52.49, H 3.92, N 7.80 %.

2.3. Single-crystal X-ray crystallography

Diffraction data for **1**·4.4H_2O·1.6EtOH, **2**·6EtOH and **3**·6EtOH were collected at 100 K on an Xcalibur PX diffractometer. All structures were refined by full-matrix least-squares techniques on F^2 with SHELXL [43]. Data collection parameters and structure solution and refinement details are listed in Table 1.

Table 1

Crystal and structure refinement data for complexes **1** – **5**

Compound reference	**1**	**2**	**3**	**4**	**5**
Chemical formula	$C_{80}H_{73}Mn_6N_{11}O_{19}$	$C_{78}H_{70.20}Mn_6N_{10}O_{19.10}$	$C_{84}H_{96}Mn_6N_6O_{24}$	$C_{82}H_{92}Mn_6N_6O_{24}$	$C_{92}H_{94}Mn_6N_6O_{28}$
Formula Mass	1822.13	1782.88	1903.31	1875.26	2061.37
Crystal system	Triclinic	Triclinic	Monoclinic	Triclinic	Triclinic
a/Å	15.080 (4)	14.435 (4)	15.999 (4)	11.650 (3)	12.123 (4)
b/Å	15.886 (5)	15.562 (5)	19.739 (5)	13.763 (4)	13.349 (4)
c/Å	18.511 (5)	19.002 (6)	14.485 (4)	15.329 (4)	16.575 (5)
α/°	101.71 (3)	104.56 (3)		94.44 (3)	101.67 (3)
β/°	109.29 (3)	107.50 (3)	112.83 (3)	111.22 (3)	110.49 (4)
γ/°	106.55 (3)	100.31 (3)		113.36 (3)	105.99 (3)
Unit cell volume/Å^3	3790 (2)	3787 (2)	4216 (2)	2032.1 (13)	2278.7 (17)
Temperature/K	100	100	100	100	100
Space group	P-1	P-1	$P2_1/c$	P-1	P-1
No. of formula units per unit cell, *Z*	2	2	2	1	1
Radiation type	Mo-Kα	Mo-Kα	Mo-Kα	Mo-Kα	Mo-Kα
Absorption coefficient, μ/mm^{-1}	1.05	1.05	0.95	0.99	0.89
No. of reflections measured	52489	45700	17846	26840	16434
No. of independent reflections	28759	25977	11086	15085	12119
R_{int}	0.024	0.029	0.024	0.022	0.037
Final R_1 values ($I > 2\sigma(I)$)	0.034	0.043	0.044	0.032	0.056
Final R_1 values (all data)	0.0583	0.0845	0.0621	0.0501	0.1052
Final $wR(F^2)$ values (all data)	0.082	0.090	0.116	0.080	0.135
Goodness of fit on F^2	1.01	1.00	1.04	1.00	1.01
CCDC	XXX	XXX	XXX	XXX	XXX

3. Results and discussion

3.1. Syntheses

The reaction between $Mn(ClO_4)_2 \cdot 6H_2O$, salicylaldoxime-like ligands and various carboxylic acids in a 1:1:1 molar ratio in basic alcoholic or acetonitrile solutions afforded hexanuclear species of general formula $[Mn^{III}_6O_2(R\text{-}sao)_6(R'\text{-}CO_2)_2(sol)_x(H_2O)_y]$ (R = H, Me and Et; R' = 1-naphthalene, 2-naphthalene and 1-pyrene; sol = MeOH, EtOH or MeCN; x = 0-4 and y = 0-4). In all five clusters, the manganese centres were found to be in the 3+ oxidation state due to the facile oxidation of Mn^{2+} to Mn^{3+} under standard aerobic conditions. Upon changing the nature of the base from NEt_3 or CH_3ONa to either NMe_4OH or NEt_4OH we did not manage to isolate any different products, as verified by pXRD measurements. Finally, repeating the same reactions under solvothermal conditions yielded an amorphous yellow precipitate in each case, which could not be further characterized and identified.

3.2. Description of structures

All five clusters (Figures 1-3) display similar but not identical structures; two $[Mn_3O(R\text{-}sao)_3]^+$ sub-units are linked together to form the final hexametallic core. Yet, there are significant differences between the seven structures. More specifically, the seven complexes may be divided in three distinct types:

Type I: complex **5** displays the "prototype" [Mn_6/oxime] structural pattern [26]. The cluster crystallizes in the triclinic P-1 space group. Its structure (Figure 1) consist of two off-set triangular $[Mn_3(\mu_3\text{-}O)(sao)_3]^+$ sub-units, which are linked *via* two O_{ox} atoms, to form a $[Mn_6(\mu_3\text{-}O)_2(sao)_6]^{2+}$ metallic core with a central $\{Mn\text{-}O_{ox}\text{-}Mn\text{-}O_{ox}\}$ rhomb between the two triangular units. The edges of each triangular sub-unit consist of $-N_{ox}\text{-}O_{ox}\text{-}$ bridges, forming a $\{Mn\text{-}N_{ox}\text{-}O_{ox}\text{-}\}_3$ ring, while the charge of the hexametallic core is counterbalanced by the presence of two *syn, syn*- η^1: η^1: μ carboxylates, with each one capping a triangular unit. The oximate ligands adopt two different coordination modes: four are found in an η^1: η^1: η^1: μ fashion, while the remaining two, responsible for the inter-triangular linkage, adopt an η^2: η^1: η^1: μ_3 coordination mode. The coordination environment of the metallic centres is completed by four terminal solvent/water molecules. Four of the six manganese centres are six-coordinate adopting

Jahn-Teller distorted octahedral geometry, while the remaining two are five-coordinate adopting square-pyramidal geometry. Finally, the two trimetallic planes, [Mn_3] and thus the JT axes, are parallel to each other.

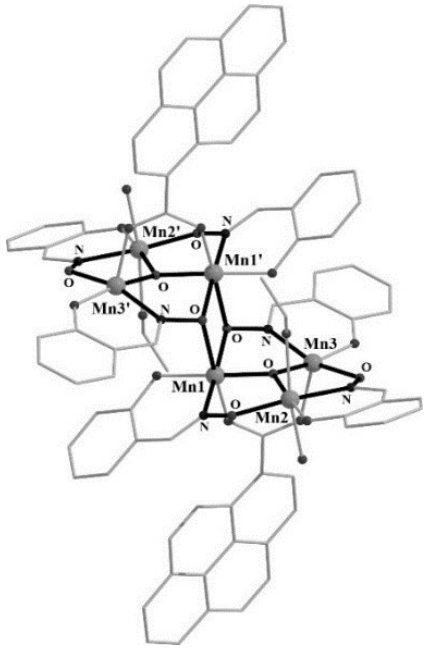

Figure 1. The molecular structure of *Type I* cluster **5**.

Type II: clusters **3** and **4** (Figure 2) display a slightly different structural motif than *Type I* clusters. The two main structural ingredients, the $[Mn_3(\mu_3\text{-}O)(R\text{-}saO)_3]^+$ sub-units, are still retained, but now two extra bridges are present arising from two O_R alkoxide groups belonging to two oximate ligands, each on a $[Mn_3(\mu_3\text{-}O)(R\text{-}sao)_3]^+$ unit. Therefore, in *Type II* clusters the inter-triangular linkage takes place *via* four bridges *vs*. two in *Type I* complexes, forming two {Mn-O_R-Mn-N_{ox}-O_{ox}} and one {Mn-O_{ox}-Mn-O_{ox}} rhombs. Furthermore, the two carboxylate ligands found in the structures are in terminal mode (*vs*. bridging in *Type I* clusters). In addition, all manganese centres are six-coordinate, with JT elongated octahedral geometry. The two [Mn_3] planes are still retained parallel to each other, as in *Type I* clusters.

Type III: clusters **1** and **2** (Figure 3) present highly distorted intermediates between *Type I* and *II* complexes. Both clusters crystallize in the triclinic P-1 space group. Again, as in *Type I*/*II* clusters, the main structural ingredients, the $[Mn_3(\mu_3\text{-}O)(sao)_3]^+$ units, are still present, but now the trimetallic planes are converging, deviating from parallel by 21.58˚ and 27.55˚ for **1** and **2**, respectively. As a result of this distortion, three main structural consequences unfold: i) a central oxo group of one triangular sub-unit is now

μ_4-O^{2-}, further bridging a manganese ion in the other [Mn_3] unit, ii) there is only one O_R alkoxide bridge from one aromatic group of an oximate ligands *vs*. two in *Type II* clusters, and iii) two long inter-triangular Mn-O_{ox} bonds are formed (~ 2.6 Å). Therefore, the bridging between the two triangular units occurs *via* five bridges *vs.* four bridges in *Type II* and two bridges in *Type I* complexes. Finally, the two carboxylate ligands are found to bond in a *syn,syn-* η^1: η^1: μ fashion. Here, we note that a similar type of complex was reported recently by *Poole et al.* [35], with the main difference in the latter complex being the presence of two μ_4-O^{2-} groups (*vs*. one in clusters **1** and **2**).

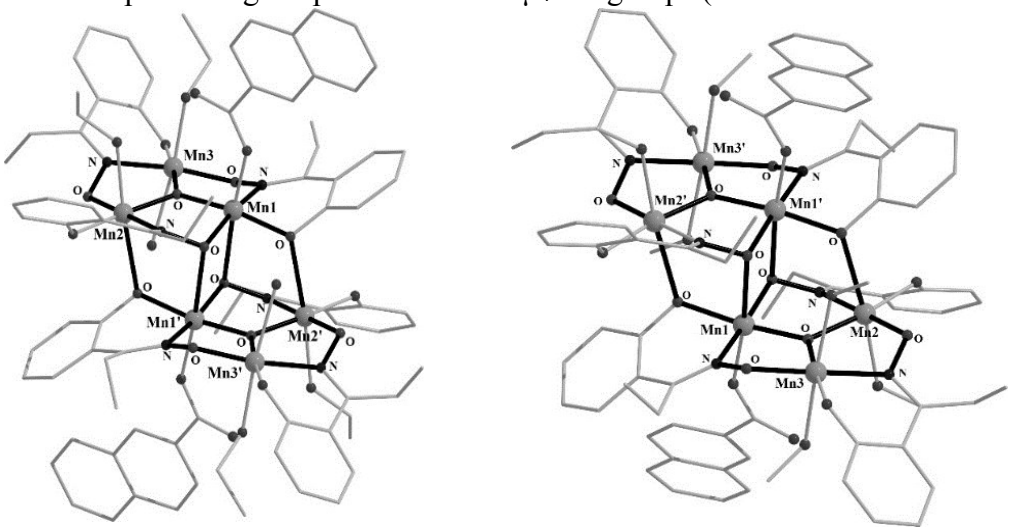

Figure 2. The molecular structures of *Type II* complexes **3** (left) and **4** (right).

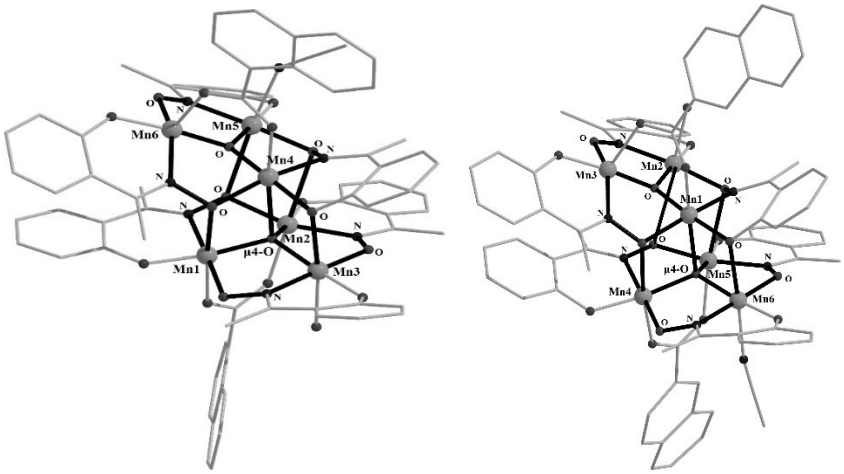

Figure 3. The molecular structures of *Type III* complexes **1** (left) and **2** (right).

In Figure 4, the metallic cores of all three types of clusters are given, and it becomes apparent that *Type I* and *Type II* complexes are closely related, while *Type III* clusters

are so distorted that the connectivity between the two triangular units is completely different.

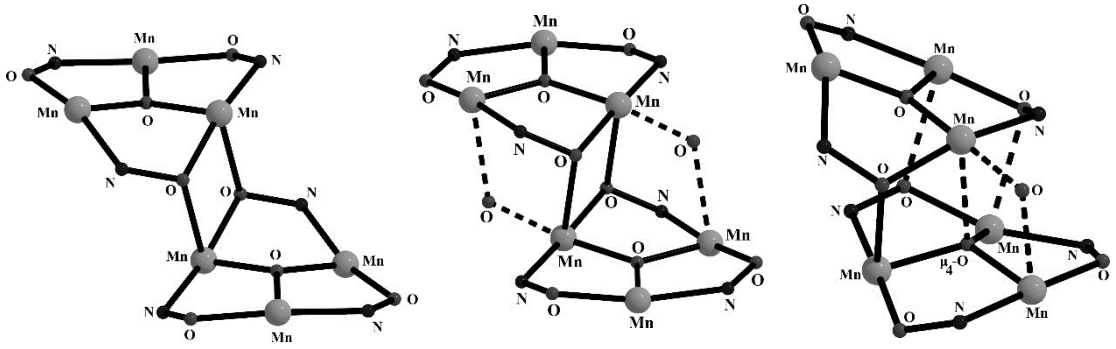

Figure 4. The metallic core of *Type I* (left), *Type II* (centre) and *Type III* (right) complexes, highlighting their main differences (dotted lines).

In the crystal the packing of *Type I* complex **5** shows six intermolecular H-bonds to the co-crystallized solvent molecules, creating chains of [Mn_6] units running along the *b* axis of the unit cell (Figure 5).

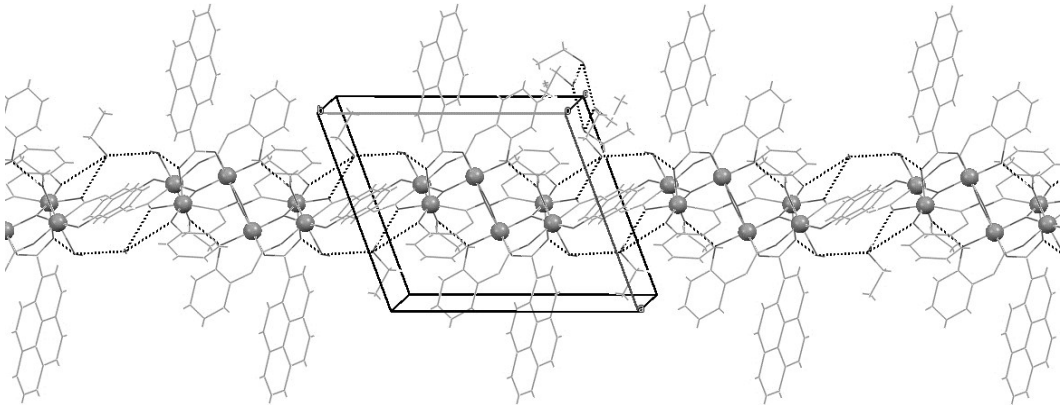

Figure 5. Crystal packing for *Type I* complex **5**, showing the inter-molecular H-bonds (dotted lines).

In the extended structures of *Type II* clusters **3** and **4** the Mn6 units stack directly upon each other forming sheets of molecules (Figure 6), while *Type III* complex **1** exhibits four inter-molecular H-bonds, creating isolated {[Mn_6]-[Mn_6]} dimers (Figure 7).

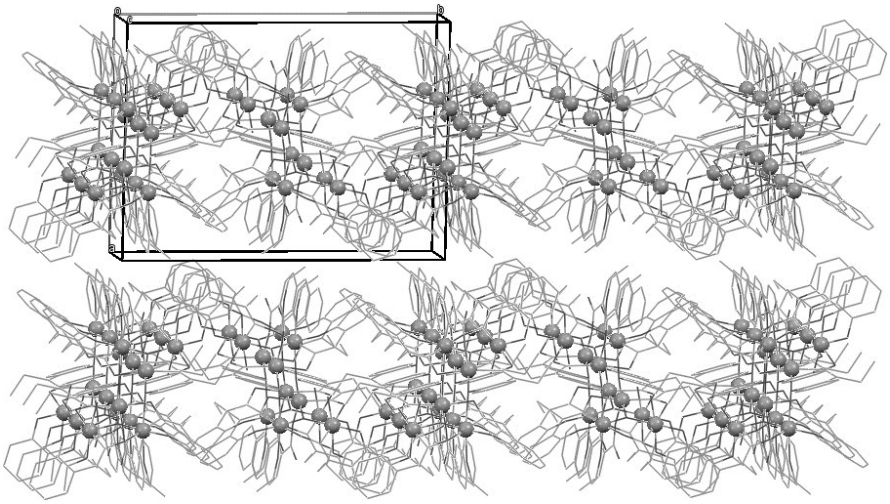

Figure 6. Crystal packing for *Type II* complex **3**.

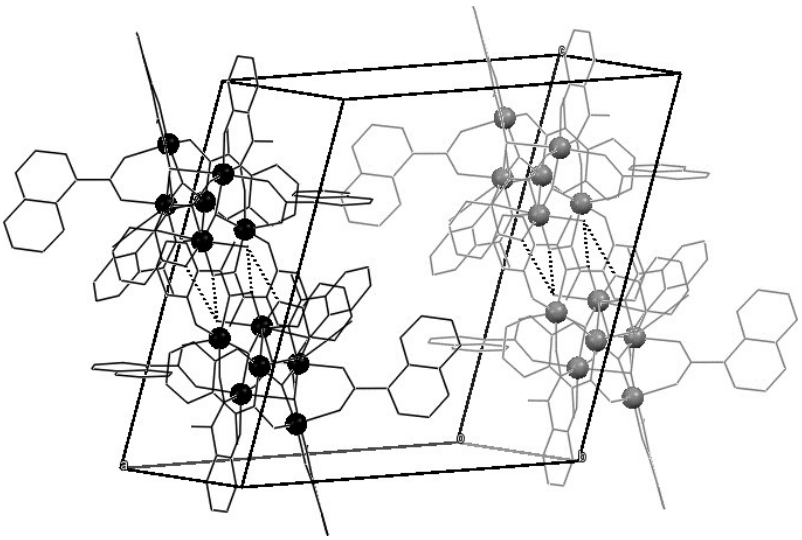

Figure 7. *Type III* {[Mn_6]-[Mn_6]} dimers in the extended structure of cluster **1**.

3.3. Magnetic properties

Dc magnetic susceptibility measurements were performed for all compounds in the 5-300 K temperature range under an applied field of 0.1 T. The results are shown as $\chi_M T$ *vs. T* plots in Figure 8.

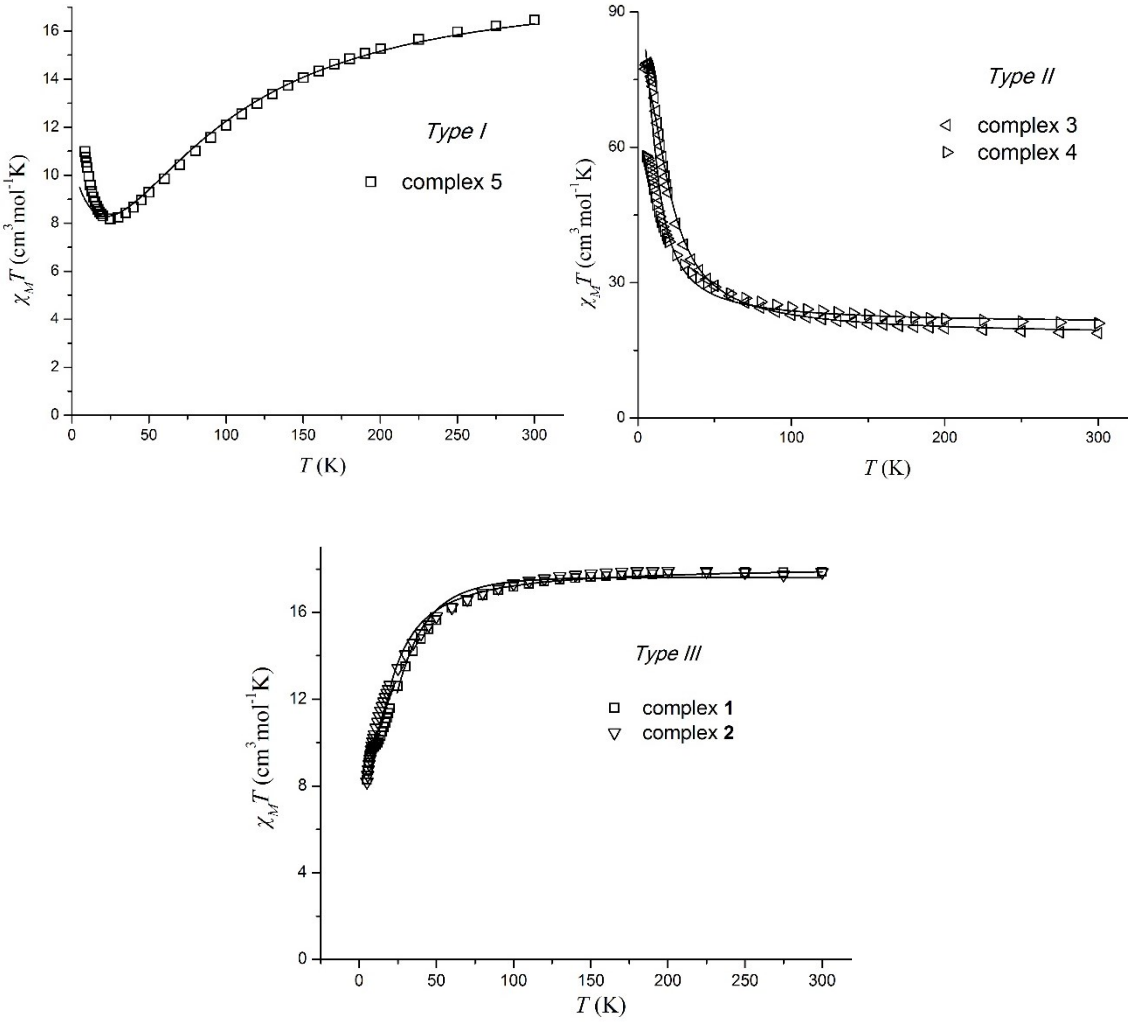

Figure 8. $\chi_M T$ *vs. T* plot for complexes **1-5** under an applied *dc* field of 1000 G. The solid lines represent simulations of the data in the 5-300 K temperature range (see text for details).

Complexes **1** and **2** display similar behaviour; the value of $\chi_M T$ decreases upon cooling suggesting the presence of dominant antiferromagnetic interactions, while in complexes **3** and **4** $\chi_M T$ increases upon cooling suggesting dominant ferromagnetic interactions. Finally, for cluster **5** the $\chi_M T$ product decreases upon cooling until ~25 K, before it increases upon further cooling. More specifically, for complexes **1** and **2**, the room temperature $\chi_M T$ values of 18.14 cm^{3}mol^{-1}K and 18.26 cm^{3}mol^{-1}K, respectively, are very close to the spin-only value of 18 cm^{3}mol^{-1}K expected for six non-interacting

Mn^{III} ions (g=2.00). Upon cooling the $\chi_M T$ value remains almost constant until ~120 K, below which it gradually decreases to reach minimum values of 8.42 $cm^3mol^{-1}K$ and 8.35 $cm^3mol^{-1}K$, for **1** and **2**, respectively. For complex **3**, the room temperature $\chi_M T$ value of 18.43 $cm^3mol^{-1}K$ slightly increases to 20.86 $cm^3mol^{-1}K$ upon cooling until ~150 K, while upon further cooling it reaches its maximum value of 77.40 $cm^3mol^{-1}K$. For complex **4**, the room temperature $\chi_M T$ value of 20.40 $cm^3mol^{-1}K$ slightly increases upon cooling to 22.58 $cm^3mol^{-1}K$ at ~150 K, before it reaches a maximum value of 58.00 $cm^3mol^{-1}K$ at 5 K. Finally, for complex **5** the room temperature $\chi_M T$ value of 16.47 $cm^3mol^{-1}K$, is smaller than the theoretical value expected for six non-interacting Mn^{III} centres (g = 2.00), indicating moderately strong antiferromagnetic interactions. Upon cooling the $\chi_M T$ value reaches its minimum value of 8.30 $cm^3mol^{-1}K$ at ~20 K, before it increases to a final value of 12.94 $cm^3mol^{-1}K$ at ~5 K.

We were able to successfully simulate the magnetic susceptibility data for all complexes, adopting two general exchange coupling schemes: i) For clusters **3**, **4** and **5** we used a scheme based on the well-established torsion angles rule, with the main parameter governing the number of J values employed in each case being the magnitude and size of the Mn-N-O-Mn torsion angle, τ (Table 3). Therefore, for cluster **5** we adopted a 2-J model (Figure 6, left). Employment of [isotropic] spin-Hamiltonian (1),

$$\hat{H} = -2J_1(\hat{S}_1\hat{S}_2 + \hat{S}_2\hat{S}_3 + \hat{S}_1\hat{S}_3 + \hat{S}_1'\hat{S}_2' + \hat{S}_2'\hat{S}_3' + \hat{S}_1'\hat{S}_3') - 2J_2(\hat{S}_1\hat{S}_4' + \hat{S}_2\hat{S}_1' + \hat{S}_1\hat{S}_2') \quad (1)$$

and using program MAGPACK [44], yielded J_1 = -7.95 cm^{-1}, J_2 = +13.80 cm^{-1} and g = 2.00. These parameters lead to a spin ground state of S = 4 for cluster **5**.

For clusters **3** and **4** we adopted a 1-J model (Figure 6, right) and spin-Hamiltonian (2),

$$\hat{H} = -2J_1(\hat{S}_1\hat{S}_2 + \hat{S}_2\hat{S}_3 + \hat{S}_1\hat{S}_3 + \hat{S}_1'\hat{S}_2' + \hat{S}_2'\hat{S}_3' + \hat{S}_1'\hat{S}_3' + \hat{S}_1\hat{S}_1' + \hat{S}_1\hat{S}_2' + \hat{S}_2\hat{S}_1') \quad (2)$$

which afforded J_1 = +1.35 cm^{-1} and g = 2.00 for complex **3**, and J_1 = +0.82 cm^{-1} and g = 2.00 for complex **4**. These parameters lead to a spin ground state of S = 12 for both complexes.

ii) For complexes **1** and **2**, which are non-classical examples of [Mn_6/oximate] clusters since they present an extra bridge through the μ_4-oxo ion, we modified the exchange coupling scheme by adding this extra feature. More specifically, for complex **1** we adopted a 3-J model (Figure 7) assuming one J_1 interaction between a) Mn1-Mn2 and

Mn2-Mn3 mediated by an μ_4-oxo bridge and an oximate ligand with Mn-N-O-Mn torsion angles of 15.95˚ and 17.73˚ respectively, b) Mn4-Mn5 and Mn5-Mn6 mediated by an μ_3-oxo bridge and an oximate ligand with torsion angles of 21.25˚ and -19.69˚ respectively, and c) Mn2-Mn6 mediated by two monoatomic O_{oxim} bridges (Mn-O_{oxim}-Mn: 95.0^o and 98.3^o); one J_2 interaction between a) Mn1-Mn3 and Mn4-Mn6 mediated by an μ_3-oxo bridge and an oximate ligand with Mn-N-O-Mn torsion angles of -33.96˚ and 39.56˚ respectively, and b) Mn1-Mn5 mediated by an oximate ligand with torsion angle of -88.13˚ (inter-triangular linkage), and one J_3 interaction between a) Mn1-Mn4 and Mn2-Mn4 mediated by an μ_4-oxo bridge and an $O_{oximate}$ bridge, and b) Mn3-Mn4 mediated by an μ_4-oxo bridge and an alkoxo group of the oximate ligand. Using the program MAGPACK and spin-Hamiltonian (3),

$$\hat{H} = -2J_1(\hat{S}_1\hat{S}_2 + \hat{S}_2\hat{S}_3 + \hat{S}_4\hat{S}_5 + \hat{S}_5\hat{S}_6 + \hat{S}_2\hat{S}_6) - 2J_2(\hat{S}_1\hat{S}_3 + \hat{S}_4\hat{S}_6 + \hat{S}_1\hat{S}_5) - 2J_3(\hat{S}_1\hat{S}_4 + \hat{S}_2\hat{S}_4 + \hat{S}_3\hat{S}_4) \quad (3)$$

afforded the parameters J_1 = -1.25 cm^{-1}, J_2 = +3.70 cm^{-1}, J_3= -1.00 cm^{-1} and g = 1.99. These parameters lead to a band of near degenerate S states of value S = 4, S = 3, S=2 and S = 1, all within ~5 cm^{-1}. Again, the ferromagnetic nature of J_2 corresponds to Mn pairs bridged by –N-O- oximate species with large torsion angles.

Finally, for complex **2** we adopted an analogous 3-*J* model (Figure 7) assuming one J_1 interaction between a) Mn1-Mn3 and Mn2-Mn3 mediated by an μ_3-oxo bridge and an oximate ligand with torsion angles of 24.78˚ and -16.42˚ respectively, b) Mn4-Mn5, Mn4-Mn6 and Mn5-Mn6 mediated by an μ_4-oxo bridge and an oximate ligand with torsion angles of -3.87˚, -29.82˚ and 20.38˚ respectively, and c) Mn5-Mn2 mediated by a monoatomic $O_{oximate}$ bridge (Mn-O_{oxim}-Mn: 100.9^o), one J_2 interaction between a) Mn1-Mn2 mediated by an μ_3-oxo bridge and an oximate ligand with torsion angle of 49.98˚, and b) Mn3-Mn4 mediated by an oximate ligand with torsion angle of -85.93˚ (inter-triangular linkage), and one J_3 between a) Mn1-Mn4 mediated by an μ_4-oxo bridge and an $O_{oximate}$ bridge, b) Mn1-Mn5 mediated by an μ_4-oxo bridge and an oximate ligand, and c) Mn1-Mn6 mediated by an μ_4-oxo bridge and an alkoxo group of the oximate ligand. Using the program MAGPACK and spin-Hamiltonian (4),

$$\hat{H} = -2J_1(\hat{S}_1\hat{S}_3 + \hat{S}_2\hat{S}_3 + \hat{S}_4\hat{S}_5 + \hat{S}_4\hat{S}_6 + \hat{S}_5\hat{S}_6 + \hat{S}_5\hat{S}_2) - 2J_2(\hat{S}_1\hat{S}_2 + \hat{S}_3\hat{S}_4) - 2J_3(\hat{S}_1\hat{S}_4 + \hat{S}_1\hat{S}_5 + \hat{S}_1\hat{S}_6) \quad (4)$$

afforded the parameters J_1 = -0.65 cm^{-1}, J_2 = +3.20 cm^{-1}, J_3= -0.8 cm^{-1} and g = 2.01. Again, as in the previous case, these parameters lead to a non-isolated spin ground-state for the cluster, since the S = 3, S= 2, S= 1 and S= 0 spin states are located within ~4 cm^{-1}. All parameters obtained from the magnetic analyses are summarized in Table 3.

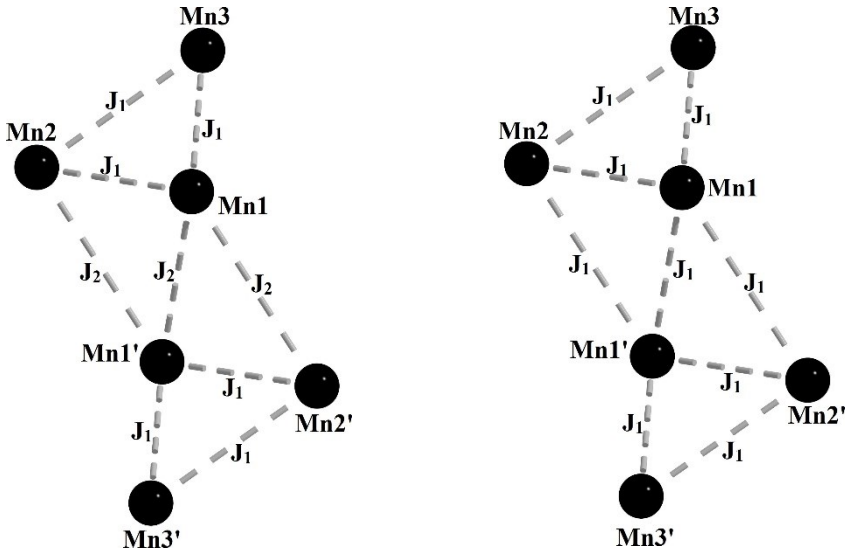

Figure 6. Exchange interaction schemes for complexes **5** (left) and **3**, **4** (right).

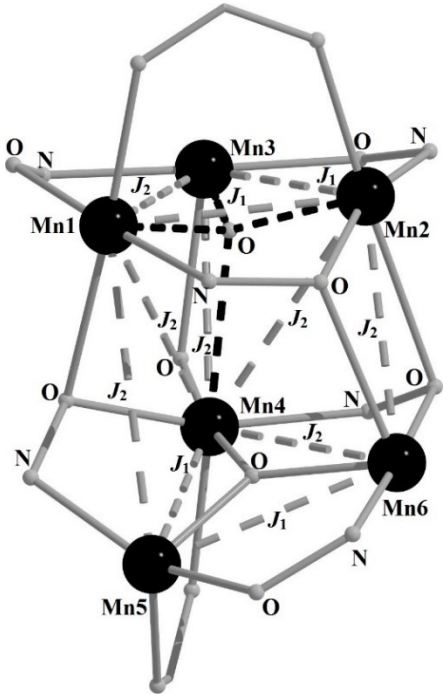

Figure 7. Exchange interaction scheme for complexes **1** and **2**.

Complexes	Torsion Angles (a°)						J coupling (cm^{-1}) ($J_1/J_2/J_3$)	g factor	Hamiltonian Equation	S, ground state	S-, 1st excited state
1·4MeCN	15.95	17.75	33.96	21.25	19.69	39.56	-1.25/+3.7/-1.0	1.99	(3)	n/a	n/a
2·3MeCN·0.1H_2O	49.98	16.42	24.78	3.87	20.38	29.82	-0.75/+3.2/-0.8	2.01	(4)	n/a	n/a
3	41.45		40.56		33.74		+1.35	2.00	(2)	12	11
4	42.77		33.29		38.48		+0.82	2.00	(2)	12	11
5·6EtOH	28.24		15.94		20.76		-7.95/+13.80	2.00	(1)	4	3

Table 3. Magnetostructural parameters for complexes **1-5**.

In order to investigate possible SMM behaviour, *ac* magnetic susceptibility measurements were carried out under zero static field in the temperature range 1.8 – 10 K with a 3.5 G ac field oscillating in the 500-1500 Hz frequency range. We chose to measure only complexes **5** and **6** due to their high spin ground-state of $S = 12$. The in-phase and out-of-phase signals are plotted as $\chi_M'T$ *vs. T* and χ_M'' *vs. T*, respectively, in Figure 9. The ac susceptibility measurements reveal features typical of SMM behaviour for both complexes. For complex **5** the $\chi_M'T$ value increases slightly upon cooling until ~5 K, indicating the presence of exited states with *S* values smaller than the ground state, before it drops rapidly to a minimum at ~4 K. Below 5 K, frequency-dependent fully formed out-of-phase (χ_M'') signals are observed. Complex **6** display similar behaviour with fully formed out-of-phase signals at ~3.5 K. The ac data of complexes **5** and **6** were fitted to the Arrhenius relationship (eq. 6),

$$\tau = \tau_0 \exp(U_{eff}/kT) \qquad (6)$$

where U_{eff} is the effective relaxation barrier, τ is the relaxation time, τ_0 is the pre-exponential factor and *k* is the Boltzmann constant, yielding $U_{eff} = 63$ K and $\tau_0 = 1.52 \times 10^{-10}$ s for complex **5** and $U_{eff} = 36$ K and $\tau_0 = 1.42 \times 10^{-8}$ s for complex **6** (Figure 10).

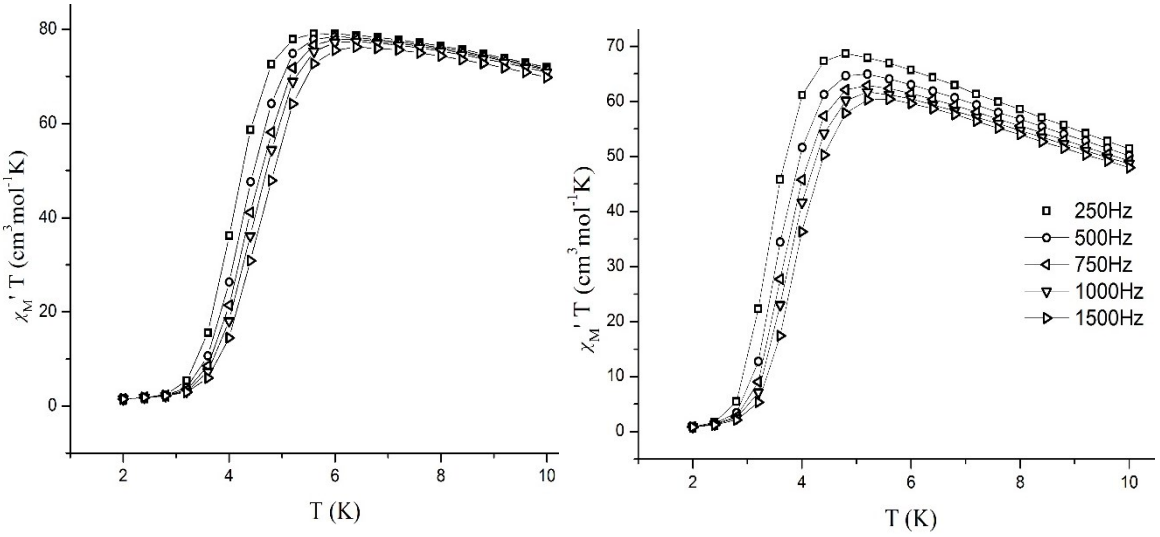

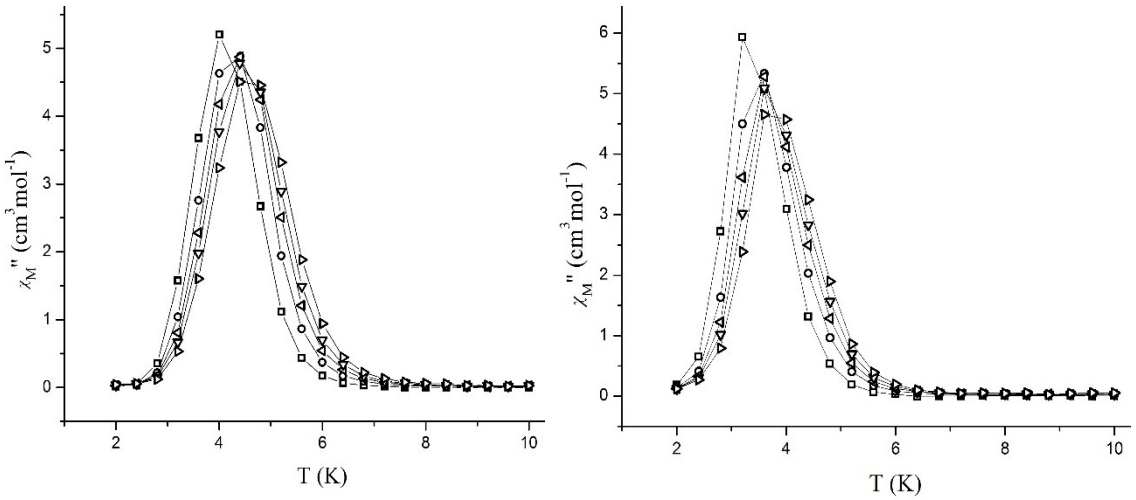

Figure 9. Plot of the in-phase signal as $\chi_M'T$ *vs. T* for complexes **5** (top, left) and **6** (top, right); plot of the out-of-phase signal as χ_M'' *vs. T* for complexes **5** (bottom, left) and **6** (bottom, right).

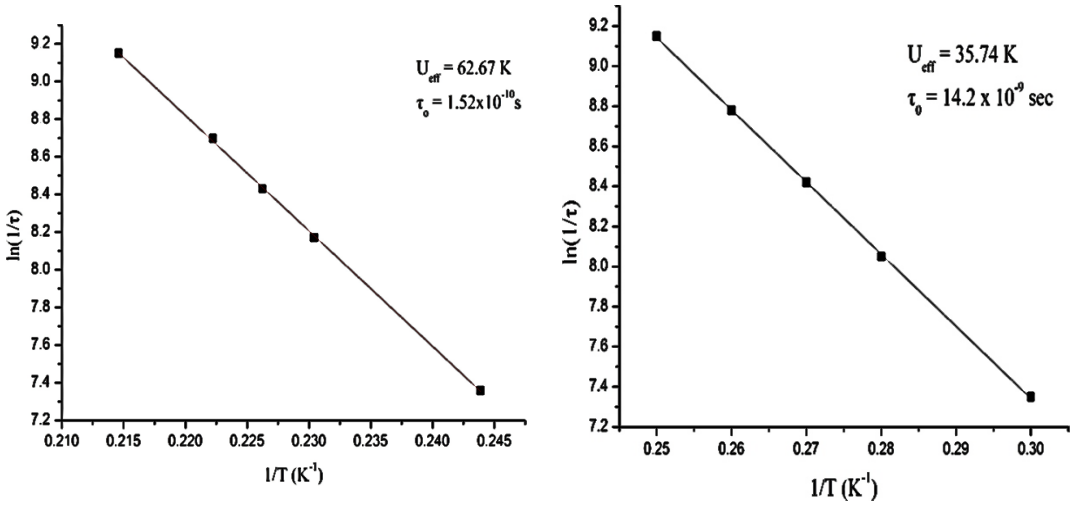

Figure 10. Arrhenius plot using powder ac magnetic susceptibility data for complexes **5** (left) and **6** (right).

4. Conclusions

In this work we have reported the synthesis and magnetic studies of seven new members of the [Mn_6/oxime] family. The use of substituted salicylaldoxime ligands, R-saoH_2 (R = H-, Me- and Et-) and carboxylate ligands, R'-CO_2H (R' = 1-naphthalene, 2-naphthalene, 9-fluorene and 1-pyrene) in manganese chemistry yielded seven complexes with formulae $[Mn_6O_2(sao)_6(1\text{-naphth-}CO_2)_2(EtOH)_4]\cdot 3EtOH$ (**1**·3EtOH); $[Mn_6O_2(sao)_6(2\text{-naphth-}CO_2)_2(H_2O)_4]$ (**2**); $[Mn_6O_2(Me\text{-sao})_6(1\text{-naphth-}CO_2)_2(H_2O)(MeCN)]\cdot 4MeCN$ (**3**·4MeCN); $[Mn_6O_2(Me\text{-sao})_6(2\text{-naphth-}CO_2)_2(H_2O)(MeCN)]\cdot 3MeCN\cdot 0.1H_2O$ (**4**·3MeCN·0.1H_2O); $[Mn_6O_2(Et\text{-sao})_6(2\text{-naphth-}$

$CO_2)_2(EtOH)_4(H_2O)_2]$ (**5**); $[Mn_6O_2(Et\text{-}sao)_6(2\text{-}naphth\text{-}CO_2)_2(MeOH)_6]$ (**6**) and $[Mn_6O_2(sao)_6(1\text{-}pyrene\text{-}CO_2)_2(H_2O)_2(EtOH)_2]\cdot 6EtOH$ (**7**·6EtOH). All clusters, besides complexes **3** and **4**, display the typical [Mn_6/oxime] core, which describes two parallel [Mn_3] planes bridged by oximate ligands. On the contrary, in complexes **3** and **4** the [Mn_3] sub-units are bridged with an extra μ_4-oxo bridge and, as such, the triangular [Mn_3] planes are converging with a deviation from the parallel arrangement of 21.58° for complex **3**, and 27.55° for complex **4**. Dc magnetic susceptibility studies for all complexes revealed dominant antiferromagnetic behaviour for complexes **1**, **2**, **3**, **4** and **7** with spin ground states of $S = 4$ for complexes **1**, **2** and **7**. For complexes **3** and **4** susceptibility data suggests the presence of a band of S states ($S \leq 4$) that are likely to be populated even at the very lowest temperatures. Complexes **5** and **6** display dominant ferromagnetic interactions between the metallic centres with spin ground states of $S = 12$. Finally, these two clusters display Single-Molecule Magnet behaviour with U_{eff} values of 62.67 K for complex **5**, and 35.74 K for complex **6**.

From these results three significant conclusions may be extracted: i) the [Mn_6/oxime] family is further extended with seven new complexes;

ii) the "torsion angle" rule is valid for the five new classical (*Type I*, *Type II*) [Mn_6/oxime] complexes. The Type III structures characterized also appear to follow this general trend, although several new analogues will need to be made to confirm this very tentative conclusions;

iii) despite more than 10 years of research into manganese-oxime cluster chemistry, new species with novel structural topologies and magnetic behavior are still uncovered, highlighting the enormously rich coordination chemistry and magnetochemistry that can be discovered via thorough investigation of synthetic space.

Supplementary material

CIF files of complexes **1**-**5**.

Acknowledgements

This work was supported by the project "IRAKLITOS II - University of Crete" of the Operational Programme for Education and Lifelong Learning 2007 - 2013 (E.P.E.D.V.M.) of the NSRF (2007 - 2013), which is co-funded by the European Union (European Social Fund) and National Resources.

References

[1] A. Caneschi, D. Gatteschi, R. Sessoli, A. L. Barra, L. C. Brunel, M. Guillot. *J. Am. Chem. Soc.*, **113**, 5873 (1991).

[2] R. Sessoli, D. Gatteschi, A. Caneschi, M. A. Novak. *Nature*, **365**, 141 (1993).

[3] SMJ. Aubin, M. W. Wemple, D. M. Adams, H-L. Tsai, G. Christou, D. N. Hendrickson. *J. Am. Chem. Soc.*, **118**, 7746 (1996).

[4] R. Sessoli, D. Gatteschi, *Angew. Chem. Int. Ed.* **42**, 268 (2003).

[5] D. Gatteschi, R. Sessoli, J. Villain, *Molecular Nanomagnets, Oxford University Press, Oxford* (2006).

[6] G. Christou, D. Gatteschi, D. N. Hendrickson, R. Sessoli, *Mater. Res. Bull.* **25**, 66 (2000).

[7] R. A. Coxall, S. G. Harris, D. K. Henderson, S. Parsons, P. A. Tasker, R. E. P. Winpenny, *J. Chem. Soc., Dalton Trans.*, 2349-2346 (2000).

[8] R. Sessoli, D. Gatteschi, *Angwe. Chem. Int. Ed*, **42**, 268 (2003).

[9] G. Aromi, E. K. Brechin, *Struct. Bond.*, **122**, 1 (2006).

[10] R. E. P. Winpenny (ed), *Single-molecule magnets and related phenomena. Struct. Bond.*, 122 (2006).

[11] R. Bagai, G. Christou, *Chem. Soc. Rev.*, **38**, 1011 (2009).

[12] A. Dei, D. Gatteschi, *Angew. Chem. Int. Ed.,* **50**, 11852 (2011).

[13] D. N. Woodruf, R. A. Layfield, *Chem. Rev.*, **113**, 5110 (2013).

[14] R. A. Layfield, *Organometallics*, **33**, 1084 (2014).

[15] G. A. Craig, M. Murrie, *Chem. Soc. Rev.*, **44**, 2135 (2015).

[16] S. K. Langley, C. Le, L. Ungur, B. Moubaraki, B. F. Abrahams, L. F. Chibotaru, K. S. Murray, *Inorg. Chem.*, **54**, 3631 (2015).

[17] L. K. Thompson, L. N. Dawe, *Coord. Chem. Rev.*, **289**, 13 (2015).

[18] S. D. Han, J. P. Zhao, S. J. Liu, X. H. Bu, *Coord. Chem. Rev.*, **289**, 32 (2015).

[19] S. Demir, I. R. Jeon, J. R. Long, T. D. Harris, *Coord. Chem. Rev.*, **289** 149 (2015).

[20] P. Happ, C. Plenk, E. Rentschler, *Coord. Chem. Rev.*, **289**, 238 (2015).

[21] D. Aravena, R. Morales, E. Ruiz, *Coord. Chem. Rev.*, **289**, 379 (2015).

[22] C. J. Milios, R. E. P. Winpenny, *Struct. Bond.*, **164**, 1 (2014).

[23] J. P. Liu, E. Fullerton, P. Guttfleisch, D. J. Sellmyer, *Nanoscale Magnetic Materials and Applications, Springer* (2009).

[24] S. Loth, S. Baumann, C. P. Lutz, D. M. Eigler, A. J. Heinrich, *Science*, **335**, 196 (2012).

[25] S. Carretta, T. Guidi, P. Santini, G. Amoretti,O. Pieper, B. Lake, J.van Slageren, W. Wernsdorfer, H. Mutka, M. Russina, C.J. Milios, E. K. Brechin. *Phys. Rev. Lett.*, **100**, 157203, (2008).

[26] C. J. Milios, C. P. Raptopoulou, A. Terzis, F. Lloret, R. Vicente, S. P. Perlepes, A. Escuer. *Angew. Chem. Int. Ed. Engl.*, **43**, 210 (2004).

[27] C. J. Milios, A. Vinslava, A. G. Whittaker, S. Parsons, W. Wernsdorfer, G. Christou, S. P. Perlepes, E. K. Brechin. *Inorg. Chem.*, **45**, 5272 (2006).

[28] C. J. Milios, A. Vinslava, P. A. Wood, S. Parsons, W. Wernsdorfer, G. Christou, S. P. Perlepes, E. K. Brechin. *J. Am. Chem. Soc.*, **129**, 8 (2007).

[29] C. J. Milios, A. Vinslava, W. Wernsdorfer, A. Prescimone, P. A. Wood, S. Parsons, S. P. Perlepes, G. Christou, E. K. Brechin. *J. Am. Chem. Soc.*, **129**, 6547 (2007).

[30] C. J. Milios, R. Inglis, A. Vinslava, R. Bagai, W. Wernsdorfer, S. Parsons, S. P. Perlepes, G. Christou, E. K. Brechin. *J. Am. Chem. Soc.*, **129**, 12505 (2007).

[31] S. Piligkos, J. Bendix, H. Weihe, C. J. Milios, E. K. Brechin. *Dalton Trans.*, 2277 (2008).

[32] U. del Pennino, V. Corradini, R. Biagi, V. De Renzi, F. Moro, D.W. Boukhvalov, G. Panaccione, M. Hochstrasser, C. Carbone, C. J. Milios, E. K. Brechin. *Phys. Rev. B,* **77**, 085419 (2008).

[33] C. J. Milios, P. A. Wood, S. Parsons, D. Foguet-Albiol, C. Lampropoulos, G. Christou, S. P. Perlepes, E. K. Brechin. *Inorg. Chim. Acta*, **360**, 3932 (2007).

[34] L. F. Jones, M. E. Cochrane, B. D. Koivisto, D. A. Leigh, S . P. Perlepes, W. Wernsdorfer, E. K. Brechin, *Inorg. Chim. Acta*, **361**, 3420 (2008).

[35] K. M. Poole, M. Korabik, M. Shiddiq, K. J. Mitchell, A. Fournet, Z. You, G. Christou, S. Hill, M. Hołyńska, *Inorg. Chem.*, **54**, 1883 (2015).

[36] D. I. Alexandropoulos, A. M. Mowson, M. Pilington, V. Bekiari, G. Christou, T. C. Stamatatos, *Dalton Trans.*, **43**, 1965 (2013).

[37] E. Manolopoulou, C. C. Stoumpos, M. Siczek, T. Lis, E. K. Brechin, C. J. Milios. *Eur. J. Inorg. Chem.*, **2010**, 483 (2010).

[38] M. Hołyńska, N. Frank, S. Dehnen. *Z. Anorg. Allg. Chem.*, **638**, 2248 (2012).

[39] R. Inglis, S. M. Taylor, L. F. Jones, G. S. Papaefstathiou, S. P. Perlepes, S. Datta, S. Hill, W. Wernsdorfer and E. K. Brechin, *Dalton Trans.*, 9157 (2009).

[40] C. J. Milios, C. Raptopoulou, A. Terzis, F. Lloret, R. Vincete, S. P. Perlepes, A. Escuer, *Angew. Chem.*, **43**, 210 (2004).

[41] C. J. Milios, A. Vinslava, W. Wernsdorfer, S. Moggach, S. Parsons, S. P. Perlepes, G. Christou, E. K. Brechin, *J. Am. Chem. Soc.*, **129**, 2754 (2007).

[42] W. R. Dunsten, T. A. Henry. *J. Chem. Soc.,* **75**, 66 (1899).

[43] G. M. Sheldrick. *Acta Crystallogr.*, ***A64***, 112 (2008).

[44] J. J. Borras-Alemnar, J. M. Clemente-Juan, E. Coronado, B. S. Tsukerblat, *J. Comp. Chem.*, **22**, 985 (2001).